View Article Online
View Journal | View Issue

Check for updates

Synthesis, nonlinear optical analysis and DFT studies of D−π−D and A−π−A configured Schiff bases derived from bis-phenylenediamine†

Rabia Farooq,[a] Zahra Batool,[a] Muhammad Khalid, ID *[bc] Muhammad Usman Khan, ID [d] Ataualpa Albert Carmo Braga, ID [e] Ahmed H. Ragab,[f] Saedah R. Al-Mhyawi,[g] Gulzar Muhammad[h] and Zahid Shafiq ID *[a]

Herein, an integral approach has been made towards the exploration of electronic and structural parameters of four synthesized (**DMA** with an A−π−A configuration and **DMM**, **DAM**, and **DMD** with a D−π−D configuration) and one designed (**DMB-D**) novel Schiff base compounds. Bis phenylenediamine derivatives were prepared by condensation of 4,5-dimethyl-*o*-phenylenediamine (**1**) with various substituted benzaldehydes (**2a–d**). The structures of compounds were confirmed by spectroscopic techniques, *i.e.*, UV-visible, FT-IR, and NMR spectroscopy. The DFT-based analysis of entitled compounds was performed *via* density functional theory utilizing the M06-2X functional in conjugation with the 6-311G(d,p) basis set to acquire geometrical parameters, natural bonding orbital (NBO), the density of states (DOS), non-linear optical (NLO), molecular electrostatic potential (MESP), and natural population analyses. The smallest band gap of (5.446 eV) was noted for **DMA** *via* frontier molecular orbital (FMO) analysis. GRPs were obtained with the aid of E_{gap} values as **DMA** with the lowest band gap displayed a small magnitude of hardness (2.723 eV) and a large magnitude of softness (0.183 eV). The β_{tot} values of **DMA**, **DMM**, **DMB-D**, **DAM**, and **DMD** were 56.95, 0.43, 2.53, 8.98, and 68.47 times larger than urea ($\beta_{tot} = 3.71 \times 10^{-31}$ e.s.u.), respectively. The observed fascinating NLO properties of these novel compounds might be helpful for further advancement in non-linear optics.

Introduction

Schiff bases are synthesized when a primary amine is treated with either a ketone or an aldehyde under certain circumstances. Schiff bases are also known as azomethine or an imine, due to the presence of the HC=N chromophore.[1,2] Schiff bases have been discovered in the biological sciences to have

[a]*Institute of Chemical Sciences, Bahauddin Zakariya University, Multan-60800, Pakistan. E-mail: zahidshafiq@bzu.edu.pk*

[b]*Institute of Chemistry, Khwaja Fareed University of Engineering & Information Technology, Rahim Yar Khan, 64200, Pakistan. E-mail: khalid@iq.usp.br; muhammad.khalid@kfueit.edu.pk*

[c]*Centre for Theoretical and Computational Research, Khwaja Fareed University of Engineering & Information Technology, Rahim Yar Khan, 64200, Pakistan*

[d]*Department of Chemistry, University of Okara, Okara-56300, Pakistan*

[e]*Departamento de Química Fundamental, Instituto de Química, Universidade de São Paulo, Av. Prof. LineuPrestes 748, São Paulo, 05508-000, Brazil*

[f]*Department of Chemistry, Faculty of Science, King Khalid University, Abha 62224, Saudi Arabia*

[g]*Department of Chemistry, College of Science, University of Jeddah, Jeddah 21419, Saudi Arabia*

[h]*Department of Chemistry, Government College University Lahore, Lahore, Pakistan*

† Electronic supplementary information (ESI) available. See DOI: https://doi.org/10.1039/d2ra05844h

antioxidant, antimalarial, antifungal, anticancer, antibacterial, anti-inflammatory, and antiviral properties, as well as catalyzing the reduction of thionyl chloride, polymerization reaction, aldol condensation reaction, reduction of ketones, hydrosilylation of ketones, Henry reaction, epoxidation of alkenes, production of bis(indolyl) methane and Diels Alder reaction.[3] A series of metal-based compounds are synthesized by using Schiff bases as ligands because they can form stable complexes with metal ions.[4,5] Schiff bases with a solvatochromic UV-vis spectrum (solvatochromicity) can serve as NLO active materials.[6] The ligands could be beneficial in solid phase extraction and the development of ion-selective electrodes for determining anions in analytical samples.[7]

The NLO compounds play an excellent part in electro-optics for signal processing, especially in fiber optics, telecommunications, and information technology.[8–10] They have simple chemistry, a low cost of creation, and a tendency to allow structural modifications to permit diverse NLO behaviors. NLO materials formed from the organic networks have become the focus of recent research.[11–13] The unique property of NLO materials is the transfer of intramolecular charge transfer (ICT) from electron donating to electron accepting moieties through conjugation links.[14–16] Experimental and computational data suggest that introducing strong donor (D) and acceptor (A) parts

on paradoxical edges of the spacer, *i.e.*, D–A, D–D–A, and A–D–A, can result in a broad second-order NLO response.[13] Charge transfer is improved in compounds containing delocalized electrons in a D–A configuration.[17,18] In optoelectronics and photonics, the demand for the production of new NLO materials has expanded dramatically in recent years. The intriguing photo-physical behavior of NLO materials, when exposed to strong laser light, is responsible for their wide range of applicability.[19,20] The synthetic organic compounds have a lot of interest in developing fast response rate, higher laser impairment approach, greater photo-electric quantum, a small value of dielectric constant, fabrication adaptability, and an inexpensive development price.

Experimental

Chemistry

All the chemicals used in this research were in extra pure form and purchased from Sigma-Aldrich. A Bruker FT-IR IFS48 spectrophotometer was used to record the FT-IR spectrum (KBr discs). On the melting point device (Büchi 434), melting points were measured. A Bruker Avance 400 spectrometer was used to capture the NMR spectrum in DMSO-d_6. The thin layer chromatographs were visualized under the influence of ultraviolet light to check the progress of reaction.

General method for the synthesis of phenylenediamine derivatives. 4,5-Dimethylbenzene-1,2-diamine (**1**) (5 mmol) was added to a stirred solution of suitable benzaldehyde (**2a–d**) (5 mmol) in 10 mL of methanol with the catalytic quantity (1–2 drops) of glacial acetic acid. The resulting mixture was allowed to cool at room temperature after being refluxed overnight and continuously monitored by the TLC. The resulting crystalline products (**DMA, DMM, DAM** and **DMD**) were filtered, cleaned with hot methanol, and allowed to air dry. The desired products with 75–90% yield were recrystallized from the methanol (Scheme 1).

The targeted compounds are characterized as follows:

(1E,1'E)-N,N'-(4,5-Dimethyl-1,2-phenylene)bis(1-(2-nitrophenyl) methanimine) (DMA). Yield 80%, mp. 156–158 °C; FT-IR (cm^{-1}): 1586 cm^{-1} (C=N), 3287 cm^{-1} (N–H), 1450 cm^{-1} (NO$_2$); ^{1}H NMR (DMSO-d_6) δ-ppm; 2.28 (s, 3H, CH$_3$), 7.06 (s, 1H), 7.73 (t, J =

7.6 Hz, 1H), 7.82 (t, J = 7.5 Hz, 1H), 8.05 (d, J = 8.0 Hz, 1H), 8.15 (d, J = 7.7 Hz, 1H), 8.76 (s, 1H, CH=N); ^{13}C-NMR (δ-ppm) 19.2, 122.0, 124.5, 129.7, 130.1, 131.9, 133.6, 135.7, 141.4, 149.3, 156.9; anal. calcd for C$_{22}$H$_{18}$N$_4$O$_4$ (402.13): C = 65.66, H = 4.51, N = 13.92; found (%): C = 65.74, H = 4.36, N = 14.01.

2,2'-((1E,1'E)-((4,5-Dimethyl-1,2-phenylene)bis(azaneylylidene)) bis(methaneylylidene))bis(4-methylphenol) (DMM). Yield 78%, mp. 157–159 °C. FT-IR (cm^{-1}): 1586 cm^{-1} (C=N), 3287 cm^{-1} (N–H), 3050 cm^{-1} (OH); ^{1}H-NMR (DMSO-d_6) δ-ppm; 2.26 (s, 3H, CH$_3$), 2.29 (s, 3H, CH$_3$), 6.85 (d, 2H, Ar-H, J = 8.4 Hz), 7.20 (s, 1H, Ar-H), 7.22 (dd, 2H, Ar-H, J = 8.4, 2 Hz), 7.43 (d, 2H, Ar-H, J = 2 Hz), 8.85 (s, 1H, CH=N), 12.81 (s, 1H, OH),; ^{13}C-NMR (δ-ppm); 19.4, 20.3, 115.6, 128.9, 129.6, 130.6, 130.9, 136.2, 140.8, 154.3, 154.9, 163.0; anal. calcd for C$_{24}$H$_{24}$N$_2$O$_2$ (372.18): C = 77.39, H = 6.50, N = 7.52; found (%): C = 77.51, H = 6.59, N = 7.67.

6,6'-((1E,1'E)-((4,5-Dimethyl-1,2-phenylene)bis(azaneylylidene)) bis(methaneylylidene))bis(2,4-di-tert-butylphenol) (DAM). Yield 90%, mp. 3.66–368 °C.; FT-IR (cm^{-1}): 1586 cm^{-1} (C=N), 3287 cm^{-1} (N–H), 3570 cm^{-1} (OH); ^{1}H-NMR (DMSO-d_6); δ-ppm; 1.29 (s, 9H, CH$_3$), 1.39 (s, 9H, CH$_3$), 2.31 (s, 3H, CH$_3$), 7.35–7.38 (m, 2H, Ar-H), 7.48 (d, 1H, J = 8.0 Hz, Ar-H), 8.97 (s, 1H, CH=N), 13.8 (s, 1H, OH); ^{13}C-NMR (δ-ppm); 19.4, 20.3, 24.1, 115.6, 116.4, 117.3, 117.6, 128.9, 130.9, 132.5, 140.8, 154.8, 168.4; anal. calcd for C$_{38}$H$_{52}$N$_2$O$_2$ (568.40): C = 80.24, H = 9.21, N = 4.92; found (%): C = 80.45, H = 9.05, N = 4.99.

4,4'-((1E,1'E)-((4,5-Dimethyl-1,2-phenylene)bis(azaneylylidene)) bis(methaneylylidene))bis(benzene-1,3-diol) (DMD). Yield 75%, mp. 315–317 °C; FT-IR (cm^{-1}): 1586 cm^{-1} (C=N), 3287 cm^{-1} (N–H); ^{1}H-NMR (DMSO-d_6); δ-ppm; 2.28 (s, 3H, CH$_3$), 6.28 (d, 1H, Ar-H, J = 2.2 Hz), 6.38 (dd, 1H, Ar-H, J = 2.2 Hz, 8.4 Hz), 7.20 (s, 1H, Ar-H), 7.42 (d, 1H, Ar-H, J = 8.4 Hz), 8.74 (s, 1H, CH=N), 12.25 (s, 1H, NH), 13.54 (s, 1H, OH); ^{13}C-NMR(δ-ppm) 19.5, 102.8, 108.1, 112.7, 120.6, 134.7, 135.7, 139.8, 162.4, 162.8, 163.8; anal. calcd for C$_{22}$H$_{20}$N$_2$O$_4$ (376.14): C = 70.20, H = 5.36, N = 7.44; found (%): C = 70.45, H = 5.31, N = 7.59.

Computational details

The DFT-based calculations of the studied compounds: **DMA, DMM, DMB-D, DAM,** and **DMD** were performed by using Gaussian 09 computational database package.[21] The obtained
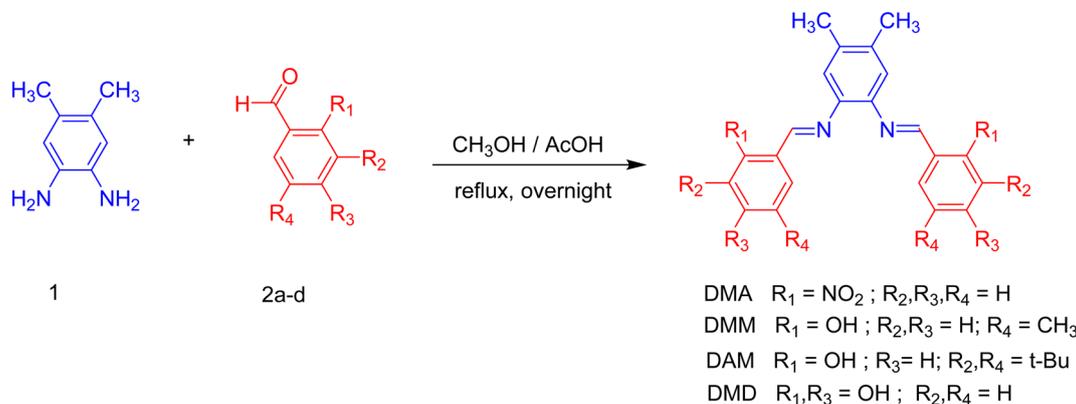
Scheme 1 Synthesis of phenylenediamine derivatives.

output files were further analyzed by GaussView,[22] Avogadro,[23] Chemcraft [24] PyMOlyze 2.0,[25] Origin 8.0,[26] and Multiwfn 3.7,[27] programs. The analysis of NBO was done by NBO 3.1 program[28] at M06-2X/6-311G(d,p). Moreover, UV-vis spectrum were studied using the same level of theory to find out the maximum wavelength of light absorbed by the compounds. Moreover, NLO characteristics (dipole moment, 1st and 2nd hyperpolarizability) along with their tensor components in x, y, and z coordinates were computed at the abovementioned functional. NPA, DOS, and MEP were also computed at the same level. The FMO inspection was executed by using the same level of DFT and the energy difference between its orbitals was utilized to compute the global reactivity indices. The dipole moment (μ),[29] average linear polarizability $\langle\alpha\rangle$, first hyperpolarizability (β_{tot}), and second hyperpolarizability γ_{tot} amplitudes were calculated by applying the given formulas[27] (eqn (1)–(4)).

$$\mu = (\mu_x^2 + \mu_y^2 + \mu_z^2)^{1/2} \tag{1}$$

$$\langle\alpha\rangle = (a_{xx} + a_{yy} + a_{zz})/3 \tag{2}$$

$$\beta_{tot} = (\beta_x^2 + \beta_y^2 + \beta_z^2)^{1/2} \tag{3}$$

where $\beta_x = \beta_{xxx} + \beta_{xyy} + \beta_{xzz}$, $\beta_y = \beta_{yxx} + \beta_{yyy} + \beta_{yzz}$ and $\beta_z = \beta_{zxx} + \beta_{zyy} + \beta_{zzz}$.

$$\gamma_{tot} = \sqrt{\gamma_x^2 + \gamma_y^2 + \gamma_z^2} \tag{4}$$

where $\gamma_i = \frac{1}{15} \sum_j (\gamma_{iijj} + \gamma_{ijij} + \gamma_{iijj})$ $i,j = \{x,y,z\}$.

Results and discussion

The structures of the synthesized Schiff bases were determined by employing microanalysis (CHN) and spectral outcomes, *i.e.*, UV-vis, FT-IR, ^{13}C-NMR, ^{1}H-NMR spectroscopy. The C=N stretching band for different compounds in FT-IR was emerged in the range of 1484–1605 cm^{-1}, whereas N–H stretching appeared in the range of 3152–3469 cm^{-1}. In ^{1}H-NMR, the O–CH$_2$ signal appeared as a quartet at δ 4.04–4.07 ppm, and CH$_3$ attached to O–CH$_2$ appeared as a triplet due to the presence of neighboring CH$_2$ at δ 1.35 ppm, while the –CH=N– signal appeared as a singlet at δ 8.70–8.90 ppm. The spectral results of other aromatic and aliphatic protons were also in correspondence with the suggested structures of the molecules in the Tables S1, S4, S7 and S10.† In this work, DFT calculations were done to obtain the NLO parameters of four different synthesized compounds: **DMA**, **DMM**, **DAM**, and **DMD** and one designed compound **DMB-D**. **DMB-D** was designed from **DAM** in order to check the effect of single tertiary butyl group over the donor region. Compound **DMA** is an A–π–A type, whereas the configuration of **DMM**, **DMB-D**, **DAM**, and **DMD** is D–π–D (see Fig. S1†). The Chemdraw structures of compounds namely ($N1E$,$N2E$)-4,5-dimethyl-N^1,N^2-bis(2-nitrobenzylidene)benzene-1,2-diamine (**DMA**), 2,2'-((1E,1'E)-((4,5-dimethyl-1,2-phenylene)bis(azanylylidene))bis(methanylylidene))bis(4-methylphenol) (**DMM**), 6,6'-((1E,1'E)-((4,5-dimethyl-1,2-phenylene)bis(azanyly-lidene))bis(methanylylidene))bis(2-($tert$-butyl)phenol) (**DMB-D**), 6,6'-((1E,1E)-((4,5-dimethyl-1,2-phenylene)bis(azanylylidene))bis(methanylylidene))bis(2,4-di-$tert$-butylphenol) (**DAM**), and 4,4'-((1E,1'E)-((4,5-dimethyl-1,2-phenylene)bis(azanylylidene))
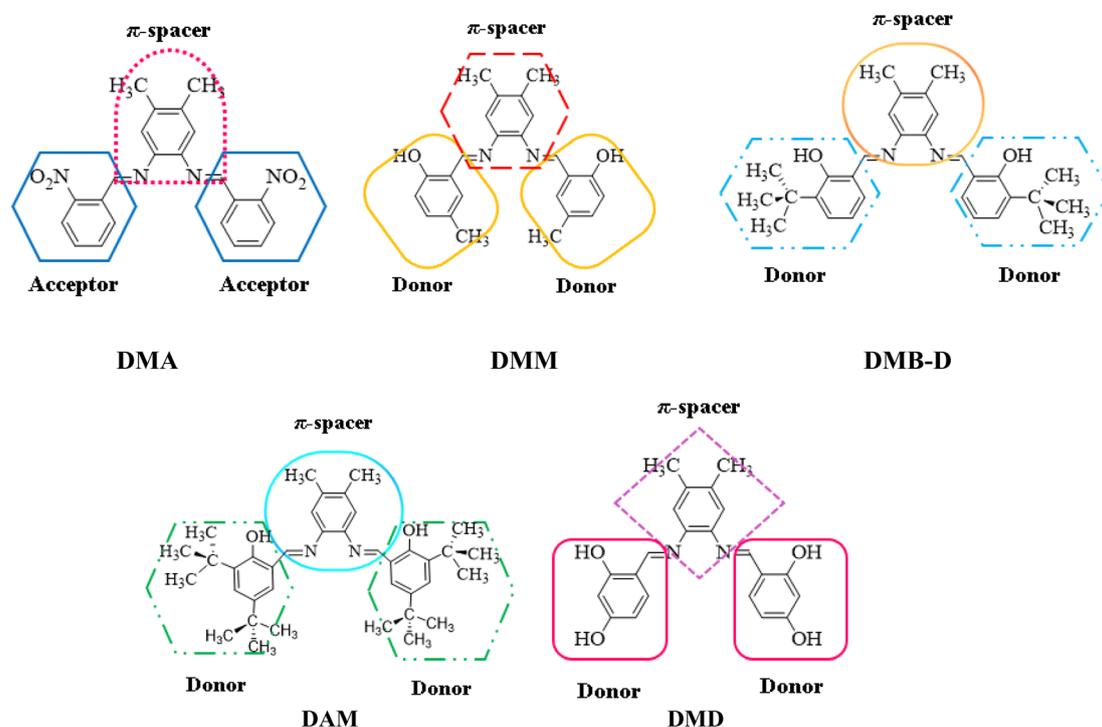
Scheme 2 A sketch map of the entitled compounds.

bis(methanylylidene))bis(benzene-1,3-diol) (**DMD**) are displayed in Scheme 2. The core unit, *i.e.*, (4,5-dimethyl-*N*1,*N*2-dimethylenebenzene-1,2-diamine) is the same in all the explored compounds, which act as π-bridge. DFT calculations were accomplished to compute the UV-vis spectrum, FMO, NBO, linear polarizability $\langle \alpha \rangle$, first hyperpolarizability (β_{tot}), and second hyperpolarizability (γ_{tot}). The energy gap had a great influence on the optical and NLO characteristics of the compounds. The consequences obtained from the computational analysis of the mentioned compounds show that these compounds are effective in non-linear optics. The chemical and optimized geometries of the investigated molecules are displayed in Fig. 1 and S13†, respectively.

Frontier molecular orbital (FMO) investigation

The energy difference in the frontier molecular orbitals is utilized to evaluate the optical polarizability, chemical response, global hardness, and softness of the examined molecules.[30,31] The HOMO is termed as a donor orbital as it is filled with electrons, while the LUMO is a partially filled or vacant orbital, which is called as an acceptor orbital.[32,33] The pictographic representation is shown in Fig. 2, and Table 1 shows the band gap values between LUMO–HOMO of the studied compounds. The $E_{HOMO} - E_{LUMO}$ gap is directly associated with the hardness (η) and chemical potential (μ) of a compound and is inversely associated with the global softness (σ) and reactivity.[34] The lesser the energy gap, the better will be the electron transport from HOMO to LUMO, and the greater will be the polarizability of the molecules.[30]

It is shown in Table 1 that the minimum band gap value (5.446 eV) is observed in **DMA**, which illustrates good intramolecular charge transfer. This excellent charge transfer in **DMA** may be found to occur due to the strong electron withdrawing effect of NO_2 attached at the acceptor site. While the maximum value of the energy gap is noted in **DMM** as 5.927 eV. The decreasing order of energy gap is **DMM** > **DMB-D** > **DMD** > **DAM** > **DMA**. Thus, **DMA** is an unstable and chemically reactive compound. It can be seen from Fig. 2 that electronic charge density is largely observed to be concentrated over the spacer region in HOMOs, whereas in the LUMO pictograph, it is found over terminal regions and partially over the spacer part, which indicates a significant charge transfer.

Global reactivity descriptors (GRDs)

The LUMO–HOMO band gap is utilized to calculate the GRDs. The results of these indices, such as ionization potential (I),[35] electron affinity (EA), global hardness (η),[36] global electrophilicity (ω),[37] electronegativity (X),[38] global softness (σ), and chemical potential (μ)[39] are estimated with the help of eqn (5)–(11), and their outcomes are tabulated in Table 2.

$$IP = -E_{HOMO} \tag{5}$$

$$EA = -E_{LUMO} \tag{6}$$

DMA

DMM

DMB-D

DAM

DMD

H C N O
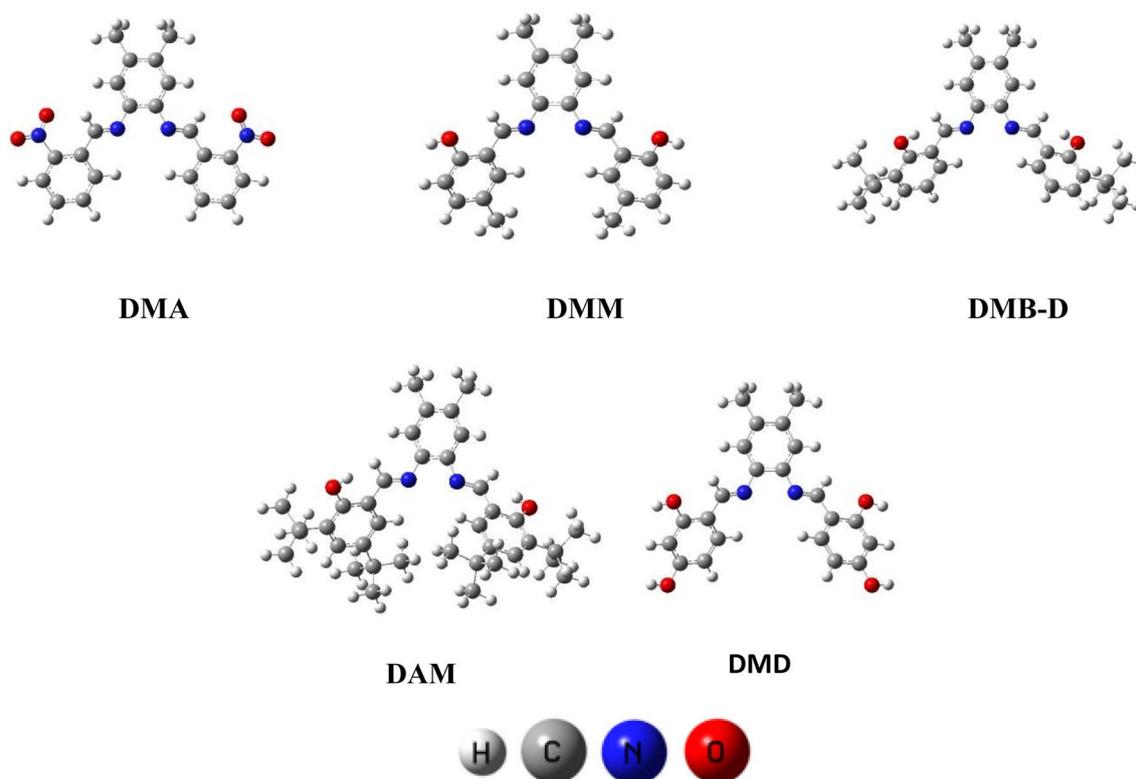
Fig. 1 Optimized geometries of the synthesized compounds.

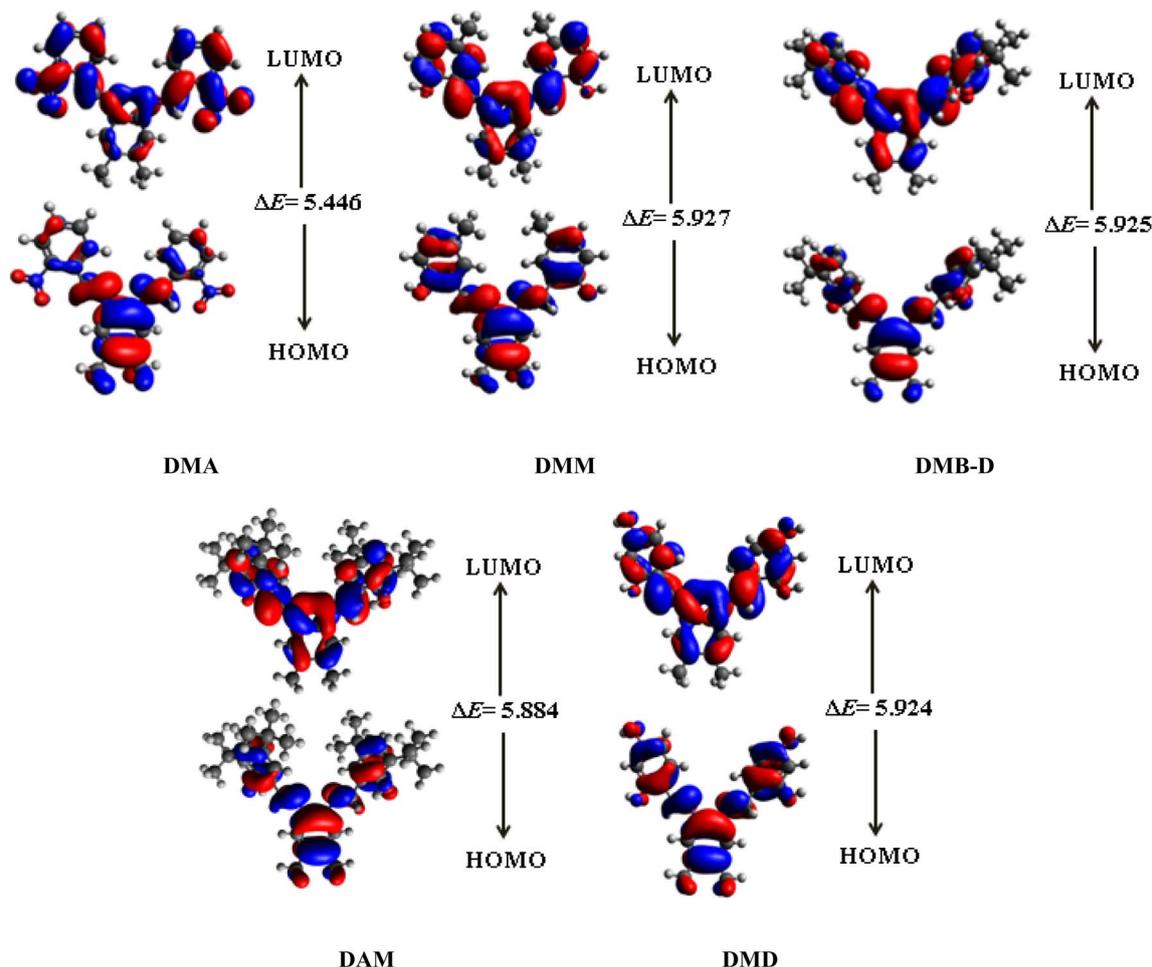© 2022 The Author(s). Published by the Royal Society of Chemistry

Fig. 2 Frontier molecular orbitals of the entitled compounds.

Table 1 HOMO/LUMO energies and band gaps of FMOs of the investigated structures[a]

Comp.	E_{HOMO}	E_{LUMO}	ΔE (eV)
DMA	−7.338	−1.892	5.446
DMM	−6.986	−1.059	5.927
DMB-D	−7.129	−1.204	5.925
DAM	−7.066	−1.182	5.884
DMD	−6.832	−0.908	5.924

[a] Units are in eV.

$$X = -\frac{[E_{\text{LUMO}} + E_{\text{HOMO}}]}{2} \qquad (7)$$

$$\eta = -\frac{[E_{\text{LUMO}} - E_{\text{HOMO}}]}{2} \qquad (8)$$

$$\mu = \frac{E_{\text{HOMO}} + E_{\text{LUMO}}}{2} \qquad (9)$$

$$\sigma = \frac{1}{2\eta} \qquad (10)$$

$$\omega = \frac{\mu^2}{2\eta} \qquad (11)$$

The electron giving and gaining the capability of molecules is calculated from their EA and IP values, respectively.[40] The ionization potential values of **DMA, DMM, DMB-D, DAM,** and **DMD** are 7.338, 6.986, 7.129, 7.066, and 6.832 eV, respectively, while electron affinity (EA) values are 1.892, 1.059, 1.204, 1.182, and 0.908 eV, respectively. The EA values of the entitled compounds are smaller than IP, which indicates that the studied compounds have greater electron-donating capacity. The highest 0.183 eV softness is shown by compound **DMA**, and the lowest 0.168 eV global softness value is exhibited by compounds **DMM, DMB-D,** and **DMD,** respectively. The overall descending order of softness is as follows: **DMA** > **DAM** > **DMM** > **DMB-D** > **DMD**. The chemical potential of the investigated compounds in declining order is **DMA** > **DMB-D** > **DAM** > **DMM** > **DMD**. Among the studied compounds, **DMA** has the greatest amplitude of electrophilicity index (3.910 eV) and **DMD** has the smallest value (2.528 eV). The electronegativity (X) values for **DMA** to **DMD** are found to be 4.615, 4.022, 4.166, 4.124 and 3.870 eV. These findings revealed that

Table 2 Global reactivity parameters of DMA, DMM, DMB-D, DAM, and DMD [a]

Comp.	IP	EA	X	η	μ	ω	σ
DMA	7.338	1.892	4.615	2.723	−4.615	3.910	0.183
DMM	6.986	1.059	4.022	2.963	−4.022	2.729	0.168
DMB-D	7.129	1.204	4.166	2.962	−4.166	2.929	0.168
DAM	7.066	1.182	4.124	2.942	−4.124	2.890	0.169
DMD	6.832	0.908	3.870	2.962	−3.870	2.528	0.168

[a] Units are in eV.

compound **DMA** has the highest softness value, which indicates that it is less stable, highly reactive and shows significant NLO response.

Natural bonding orbital (NBO) analysis

The NBO approach is utilized to observe the electronic charge transference phenomenon from electron donating to electron accepting moieties, hyper conjugative and non-covalent interactions (inter and intra-molecular hydrogen bonding) in the molecule. The second-order perturbation energy is calculated by using eqn (12).

$$E^{(2)} = q_i \frac{F(i,j)^2}{\varepsilon_j - \varepsilon_i} \tag{12}$$

where, $E^{(2)}$ represents stability energy, $\varepsilon_j - \varepsilon_i$ indicates diagonal elements, q_i depicts orbital occupancy, and $F(i,j)$ shows off-diagonal NBOs Fock matrix components.[41] The NBO analysis of the studied compounds is performed via using the above-mentioned functional and some of its outcomes are displayed in Table 3, while rest of the transitions are added in Tables S1–S4.†

Generally, four major kinds of electronic transitions are observed, i.e., σ → σ*, π → π*, LP → σ*, and LP → π*. π → π* is found to be the most probable electronic transition. From these, π(C21–C22) → π*(C23–C24), π(C20–C21) → π*(C22–C23), π(C28–C29) → π*(C27–C32), π(C1–C6) → π*(C4–C5), and π(C22–C23) → π*(C19–C24) have stabilization energy values of 34.52, 32.90, 30.73, 29.93, and 36.31 kcal mol^{-1} in **DMA**, **DMM**, **DMB-D**, **DAM** and **DMD** respectively. The transitions likeπ(N46–O48) → π*(C28–C29), π(N17–C49) → π*(C19–C24), π(N17–C37) → π*(C19–C24), π(C19–C28) → π*(C19–C24), and π(C17–C39) → π*(C19–C24) with energy values of 2.90, 8.23, 7.80, 7.93, and 7.97 kcal mol^{-1} are observed in **DMA**, **DMM**, **DMB-D**, **DAM** and **DMD**, accordingly. These are the lowest stability energy amplitudes among all the π → π* transitions in the examined compounds. Likewise, σ(C19–C20) → σ*(C24–N43), σ(O47–H48) → σ*(C28–C33), σ(C20–H25) → σ*(C19–C24), σ(C20–H25) → σ*(C19–N24), and σ(O37–H38) → σ*(C27–C32) transitions are observed with a maximum

Table 3 Natural bond orbital (NBO) analysis of the entitled compounds

Comp.	Donor (i)	Type	Acceptor (j)	Type	$E^{(2)}$ [kcal mol^{-1}]	$E(j) - E(i)$ (a.u.)	$F(i,j)$ (a.u.)
DMA	C19–C20	σ	C24–N43	σ*	5.89	1.11	0.073
	C28–C33	σ	C28–N46	σ*	0.53	1.14	0.022
	C21–C22	π	C23–C24	π*	34.52	0.34	0.097
	N46–O48	π	C28–C29	π*	2.90	0.59	0.041
	O44	LP(3)	N43–O45	π*	214.63	0.22	0.197
	O47	LP(2)	C28–C29	σ*	0.65	1	0.023
DMM	O47–H48	σ	C28–C33	σ*	5.72	1.46	0.082
	C5–H8	σ	C4–N17	σ*	0.53	1.1	0.022
	C20–C21	π	C22–C23	π*	32.90	0.35	0.096
	N17–C49	π	C19–C24	π*	8.23	0.45	0.060
	O45	LP(2)	C19–C24	π*	33.66	0.46	0.120
	O45	LP(1)	C19–C24	σ*	0.55	1.31	0.024
DMB-D	C20–H25	σ	C19–C24	σ*	5.06	1.21	0.070
	C22–C23	σ	C43–C48	σ*	0.51	1.21	0.022
	C28–C29	π	C27–C32	π*	30.73	0.35	0.094
	N17–C37	π	C19–C24	π*	7.80	0.45	0.058
	O35	LP(2)	C19–C24	π*	29.12	0.46	0.112
	O36	LP(1)	C27–C28	σ*	0.50	1.29	0.023
	C20–H25	σ	C19–C24	σ*	5.03	1.21	0.070
	C22–C23	σ	C41–C42	σ*	0.52	1.21	0.022
	C1–C6	π	C4–C5	π*	29.93	0.34	0.091
DAM	C19–C28	π	C19–C24	π*	7.93	0.46	0.059
	O35	LP(2)	C19–C24	π*	29.10	0.46	0.112
	O36	LP(1)	C27–C28	σ*	0.50	1.29	0.023
DMD	O37–H38	σ	C27–C32	σ*	5.62	1.46	0.081
	C2–H7	σ	C3–N18	σ*	0.52	1.1	0.021
	C22–C23	π	C19–C24	π*	36.31	0.36	0.105
	C17–C39	π	C19–C24	π*	7.97	0.37	0.012
	O45	LP(2)	C22–C23	π*	38.03	0.45	0.125
	O45	LP(1)	C21–C22	σ*	0.55	1.3	0.024

magnitude as 5.89, 5.72, 5.06, 5.03, and 5.62 kcal mol^{-1} in **DMA**, **DMM**, **DMB-D**, **DAM** and **DMD**, respectively. Similarly, σ(C28–C33) → σ*(C28–N46), σ(C5–H8) → σ*(C4–N17), σ(C22–C23) → σ*(C43–C48), σ(C22–C23) → σ* (C41–N42), and σ(C2–H7) → σ*(C3–N18) transitions with the lowest energy values of 0.53, 0.53, 0.51, 0.52, and 0.52 kcal mol^{-1} are detected in **DMA**, **DMM**, **DMB-D**, **DAM** and **DMD**, correspondingly.

Furthermore, the most prominent LP → π* transitions are LP3(O44) → π*(N43–O45), LP2(O45) → π*(C19–C24), LP2(O35) → π*(C19–C24), LP2(O35) → π*(C19–C24), and LP2(O45) → π*(C22–C23) with 214.63, 33.66, 29.12, 29.10, and 38.03 kcal mol^{-1} stabilization energy. Similarly, LP2(O47) → σ*(C28–C29), LP1(O45) → σ*(C19–C24), LP1(O36) → σ*(C27–C28), LP1(O36) → σ*(C27–C28), and LP1(O45) → σ*(C21–C22) manifested minimum energy of 0.65, 0.55, 0.50, 0.50, and 0.55 kcal mol^{-1}, correspondingly. Some other electronic transitions are also observed, which are presented in the Tables S1–S4.† The NBO investigation disclosed the delocalization of electrons and hyper conjugative interactions, which in turn cause ICT, are the foremost reasons for the stability of the molecule and are crucial for good NLO response.

Density of states (DOS)

The scattering of electronic clouds on different parts of the compound is studied with the help of DOS. To obtain the DOS graph, we made fragments of our compounds, *i.e.*, acceptor, π-spacer (linker) in **DMA** and donor, π-linker in **DMA**, **DMM**, **DMB-D**, and **DMD**. The PDOS (partial density of states) and TDOS (total density of states) graphs of the synthesized compounds are examined and presented in Fig. 3. In **DMA**, the contribution of 85.6% is made by the acceptor to LUMO, while it
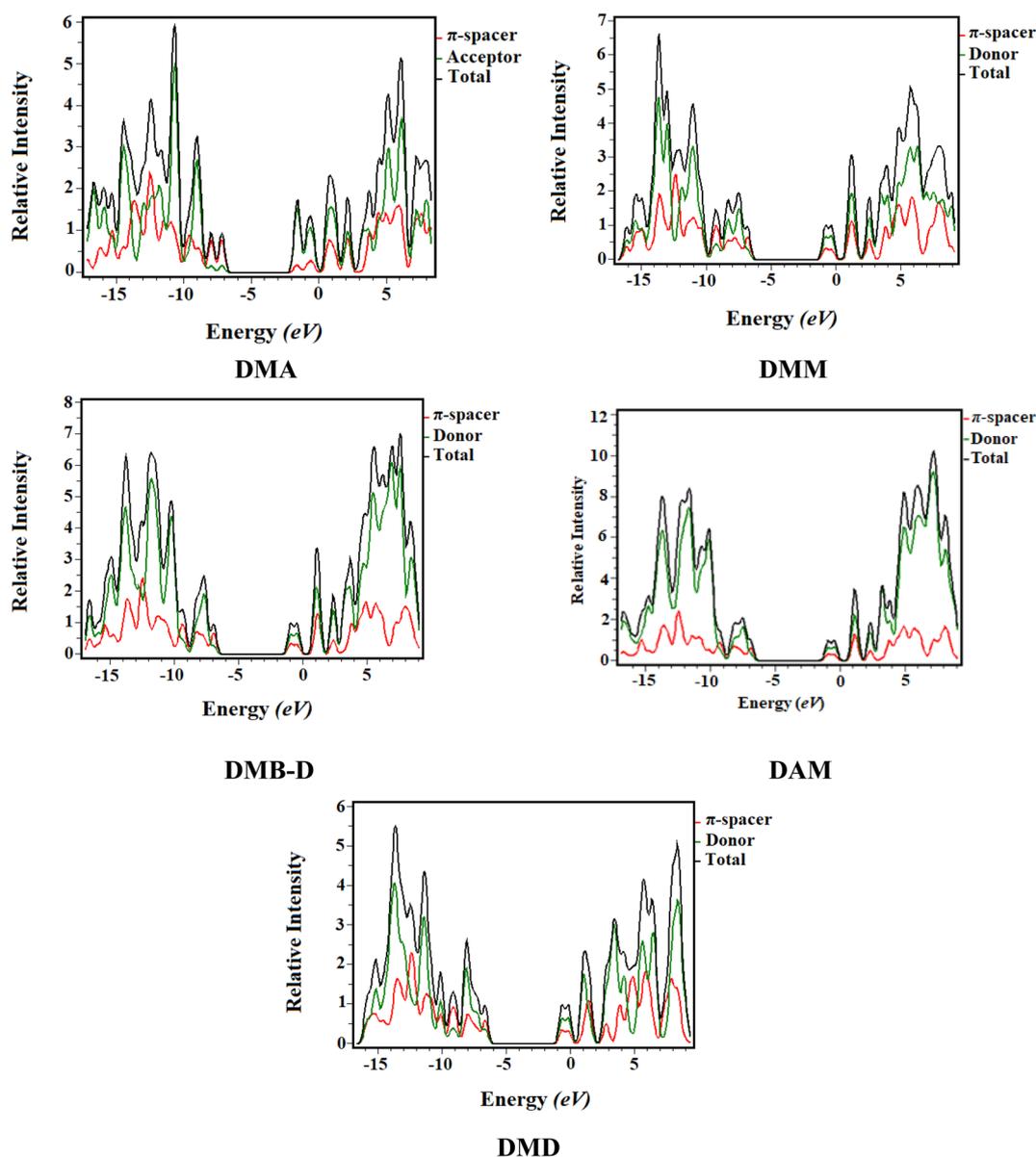

Fig. 3 Graphical representation of DOS for the entitled compounds.

contributes 18.2% to HOMO, whereas the π-spacer shows 14.4% of its involvement to LUMO and 81.8% to HOMO. In the cases of **DMM**, **DMB-D**, **DAM** and **DMD**, the donor contributes 66.6, 64.9, 65.2, and 64.9% to LUMO, while a contribution of 30.3, 28.5, 34.4 and 37.6%, respectively and is observed towards HOMO. The π-spacer depicts a 33.4, 35.1, 34.8, and 35.1% contribution pattern to LUMO, while 69.7, 71.5, 62.4, and 65.6% towards HOMO from **DMM**, **DMB-D**, **DAM** and **DMD**, correspondingly (Table S14†). In the synthesized molecule **DMA**, most of the electron density is present on the π-spacer in HOMO, whereas in LUMO it is more concentrated on the acceptor part. The other synthesized molecules have identical patterns of distribution of electron density as HOMO has electron density on π-linker (4,5-dimethyl-N^1,N^2-dimethylenebenzene-1,2-diamine), while LUMO has more density on the donor and a little bit is present on π-linker.
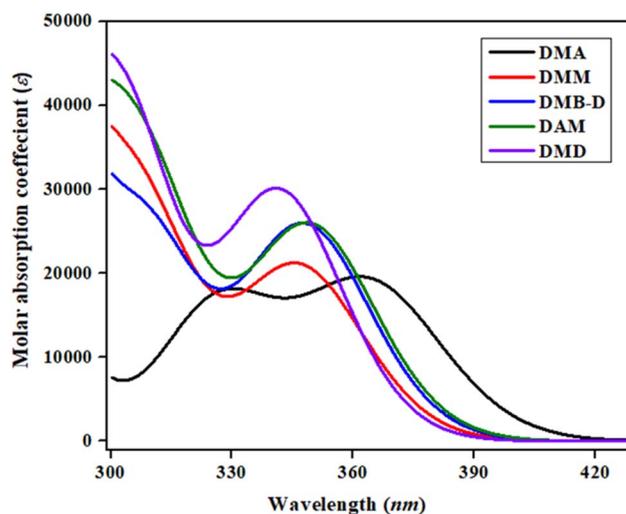
UV-vis analysis

UV-vis analysis provides significant information regarding the charge transfer capability, nature of transitions, and phenomenon of absorption in the synthesized compounds (**DMA**, **DMM**, **DMB-D**, **DAM**, and **DMD**).[42] TD-DFT is employed to calculate the photophysical characteristics of **DMA**, **DMM**, **DMB-D**, **DMB**, and **DMD** using the dichloromethane (DCM) solvent. The maximum wavelength (λ_{max}) of light absorbed, excitation energy (E), molecular orbital (MO) contributions, and oscillator strength (f) of the studied molecules are calculated by the same technique of TD-DFT and the outcomes are represented in Table 4, whereas, results of other molecular orbital contributions are displayed in Tables S5–S9.†

It is observed from the results that transition energy is inversely proportional to λ_{max} and directly related to oscillation strength. As the excitation energy value and oscillation strength increase, the wavelength of absorption maxima decreases. Therefore, the highest λ_{max} value of 364.068 nm was obtained in **DMA** with 3.405 eV excitation energy and 0.254 oscillation strength. Hence, it showed a bathochromic shift. Remarkably, the highest value of λ_{max} in **DMA** is due to the existence of strong electron withdrawing (–NO$_2$) groups, which decrease the energy gap ($E_{HOMO} - E_{LUMO}$). An appreciable decrease in the value of λ_{max} is observed in **DMB-D** (347.811 nm). The minimum value of λ_{max} value is 341.477 nm, as observed in **DMD**. The descending trend of λ_{max} of the investigated molecules is as follows: **DMA** > **DAM** > **DMB-D** > **DMM** > **DMD** (Fig. 4).

Fig. 4 Absorption spectrum of DMA, DMM, DMB-D, DAM, and DMD.

Natural population analysis (NPA)

The electronic cloud distribution on an atom has a great impact on the chemical reactivity, dipole moment, and electrostatic interaction between the atoms and molecules, and many other properties of the chemical system. The effective calculation of the atomic charge of the titled compounds is essential for a better understanding of the conjugated system.[43,44] The Mulliken charges of **DMA**, **DMM**, **DMB-D**, **DAM** and **DMD** were calculated at the aforementioned level and are presented in Fig. 5.

The charge density distribution revealed that the nitrogen atoms associated with oxygen in **DMA** are positively charged, whereas those attached to carbon and hydrogen in all of the titled compounds are negatively charged. Moreover, all the hydrogen atoms are positively charged. The oxygen atoms linked with carbon and hydrogen atoms are negatively charged. All the nitrogen atoms present in the π-linker are negatively charged (see Fig. 5). The overall analysis of Mulliken charges revealed that the unequal distribution of charges on the entitled compounds is because of the nitrogen and oxygen atoms.

Molecular electrostatic potential (MEP)

The MEP plot is widely used to predict electrostatic potential, chemical reactivity, electrophilic, and nucleophilic attacks on the reactive site in a molecular system. The MEP diagram is mapped over the optimized structure of the molecule to signify the overall electron density. The different colors are utilized to designate the electrostatic potential over the MEP surface, shown in Fig. 6. The enhancing trend of potential is: red < orange < yellow < green < blue.[45,46] The MEP plot displayed that most of the red color is on oxygen atoms, which showed the probability of electrophilic attack. Although most of the green and blue bands which elucidate positive potential are positioned on carbon and hydrogen atoms that are efficient for nucleophilic reactions.

Table 4 Excitation energy (E), oscillator strength (f), and wavelength (λ) and of studied molecules[a]

Comp.	DFT λ (nm)	E (eV)	f	MO contributions
DMA	364.068	3.405	0.254	H → L(67%), H−1 → L+1(2%)
DMM	346.196	3.581	0.286	H → L(77%), H−1 → L+1(3%)
DMB-D	347.811	3.564	0.352	H → L(79%), H−1 → L+1(3%)
DAM	348.956	3.553	0.353	H → L(77%), H−1 → L+1(3%)
DMD	341.477	3.631	0.408	H → L(79%), H−1 → L+1(4%)

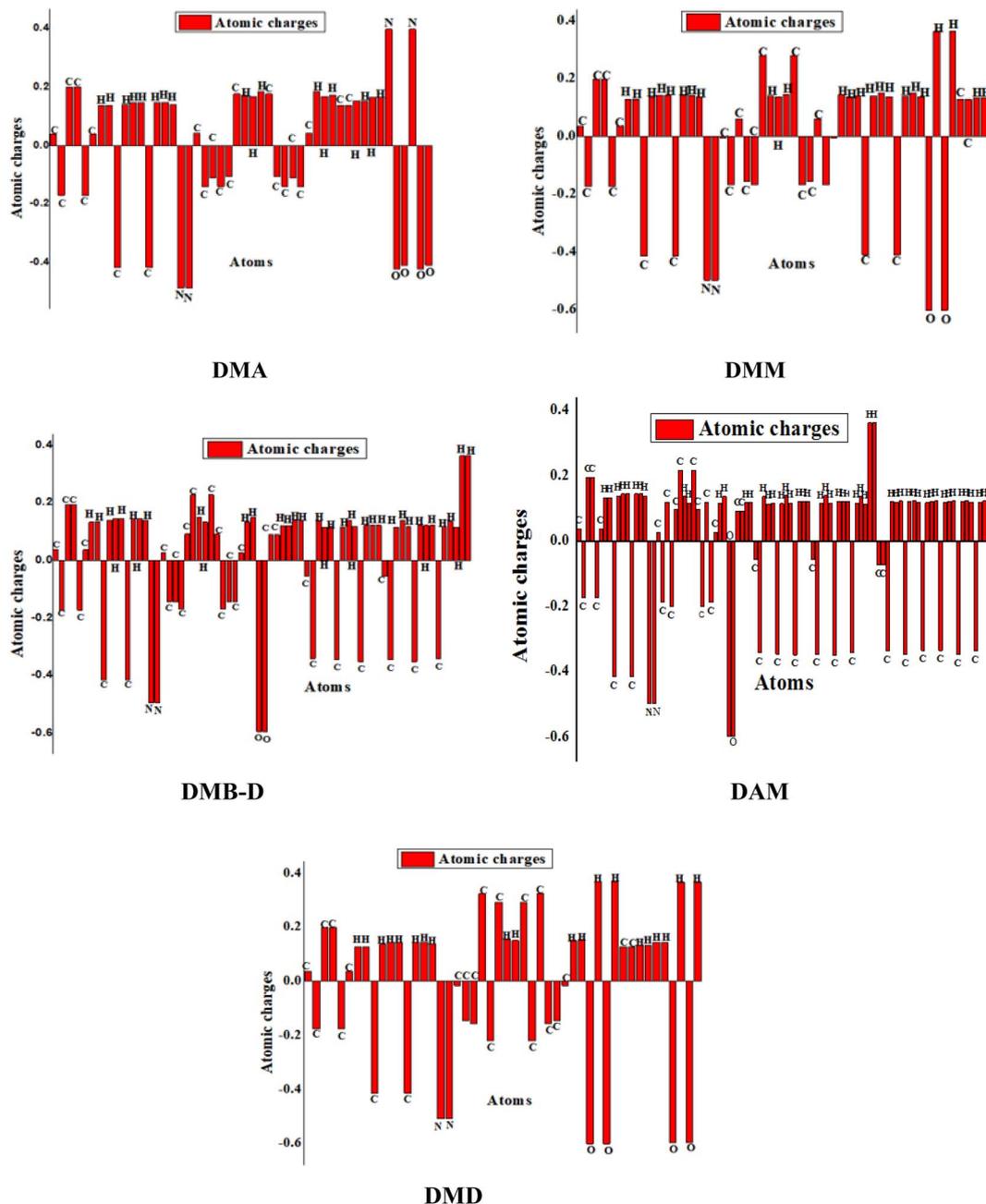[a] MO = molecular orbital, H=HOMO, L = LUMO, f = oscillator strength.

Fig. 5 Natural population analysis of DMA, DMM, DMB-D, DAM, and DMD.

Non-linear optical (NLO) properties

The materials that display NLO properties have become an extensive research discipline because of their widespread applications in optoelectronics, telecommunication, and optical switches.[47] The dipole moment (μ) and hyperpolarizability (β_{tot} and γ_{ot}) display the electronic communication in different fragments of the molecule.[48] The data computed for dipole moment (μ), average polarizability and hyper polarizabilities (β_{tot} and γ_{tot}) are tabulated in Table 5 while the major contributing tensors are presented in Tables S10–S13.†

The utmost value of μ_{tot} (2.385 D) is viewed in **DMA** while the least possible value (0.202 D) is noticed in **DMD**. For a better analysis of NLO behavior, the dipole moment and first hyperpolarizability of the studied compounds are compared with the urea molecule, which has been regarded as a standard molecule in the literature study. The dipole moment of **DMA** is greater than urea (1.3732 D),[42] while **DMM**, **DMB-D**, **DAM**, and **DMD** have smaller dipole moment values than urea.

The highest value of first-order polarizability (877.438 × 10^{-25} e.s.u.) is noted for compound **DAM**, whereas the lowest value (549.863 × 10^{-25} e.s.u.) is examined for compound **DMD** among the remaining synthesized compounds. The overall
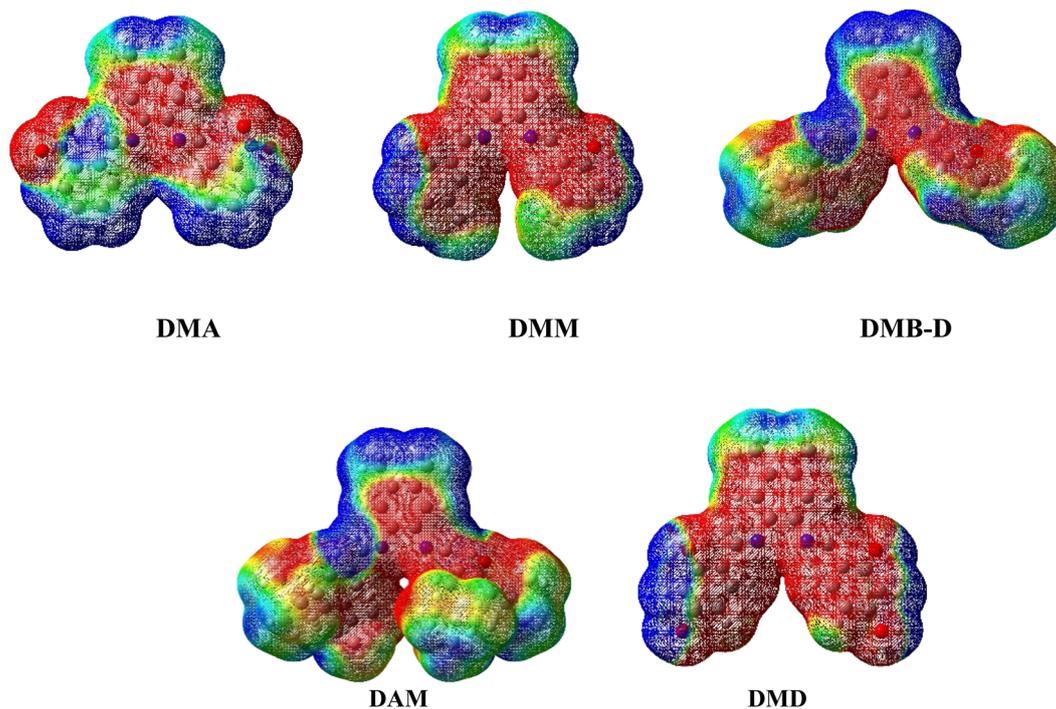
DMA **DMM** **DMB-D**

DAM **DMD**

Fig. 6 MEP representation of the entitled compounds.

Table 5 The, average polarizability, dipole moment, first hyper-polarizability, second hyperpolarizability results for investigated molecules[a]

Comp.	μ_{tot}	$\langle\alpha\rangle \times 10^{-25}$	$\beta_{tot} \times 10^{-33}$	$\gamma_{tot} \times 10^{-35}$
DMA	2.385	561.702	21 129.545	20.761
DMM	0.705	566.066	161.594	17.170
DMB-D	0.882	700.910	942.348	19.320
DAM	0.659	877.438	3335.274	21.239
DMD	0.202	549.863	25 438.874	20.373

[a] μ_{tot} has a unit in D, while $\langle\alpha\rangle$, β_{tot} and γ_{tot} have units in e.s.u.

decreasing trend of $\langle\alpha\rangle$ is in the following order: **DAM** > **DMB-D** > **DMM** > **DMA** > **DMD**. The $\langle\alpha\rangle$ of the titled compounds is more dominant along the y-direction, which means that polarization predominantly takes place in the y-direction. The linear polarizability in α_{xx}, α_{yy}, and α_{zz} directions is 981.133, 983.541, and 667.438 $\times 10^{-25}$ e.s.u., correspondingly in **DAM**, which is the highest than the linear polarizability of other entitled compounds as shown in Table S11.† The lowest values of dipole polarizability in x, y, and z-direction are 675.571, 716.639, and 257.399 $\times 10^{-25}$ e.s.u., respectively, observed in **DMD**.

In first hyperpolarizability (β_{tot}), the tensor β_{xxy} has the major contribution in β_{tot} value with 12 747.514 $\times 10^{-33}$ e.s.u. amplitude in **DMA** while in **DMM**, **DMB-D**, **DAM**, and **DMD** the major involvement of β_{tot} is made by β_{yzz} (160.102, 6.038, 1176.196, and 380.946 $\times 10^{-33}$ e.s.u.), respectively. The declining trend β_{tot} values are: **DMD** > **DMA** > **DAM** > **DMB-D** > **DMM**. A comparative study of β_{tot} of the studied compounds with urea showed that the values of β_{tot} of **DMA**, **DMM**, **DMB-D**,

DAM, and **DMD** are 56.87, 0.43, 2.53, 8.98, and 68.47 times larger than urea ($\beta_{tot} = 3.71 \times 10^{-31}$ e.s.u.),[49] correspondingly.

Moreover, compound **DAM** shows the largest 21.239 $\times 10^{-35}$ e.s.u. second hyperpolarizability (γ_{tot}) value, and the smallest value of γ_{tot} 19.320 $\times 10^{-35}$ e.s.u., is depicted by compound **DMM**. The γ_{tot} values of other synthesized compounds are in the following order: **DAM** > **DMA** > **DMD** > **DMB-D** > **DMM**. In the case of the second hyperpolarizability, the greatest involvement of tensor γ_y is observed for compound **DMM** with a value of 9.181 $\times 10^{-35}$ e.s.u. However, the tensor γ_z has a minor contribution in γ_{tot} value with an amplitude of 0.228 $\times 10^{-35}$ e.s.u. examined in compound **DMM**. From the above discussion, it is predicted that because of the higher values of dipole moment and first hyperpolarizability compound, **DAM** might act as an excellent NLO material.

Conclusion

In the present work, 4,5-dimethyl-o-phenylenediamine based Schiff base compounds (**DMA**, **DMM**, **DMB-D**, **DAM**, and **DMD**) were synthesized and computationally analyzed to investigate their NLO characteristics. The highest bathochromic shift (λ_{max} = 364.068 nm) was shown by **DMA** as compared to other compounds. The band gap was lowered from 5.927 to 5.446 eV and among all the compounds, the lowest E_{gap} was found in **DAM** (5.446 eV), which revealed a good transfer of charge within the molecule. However, in the case of NLO analysis, there was an enhancement in the β_{tot} value (25 438.874 $\times 10^{-33}$ e.s.u.) of **DMA** as compared to other molecules. The $\sigma \rightarrow \sigma^*$ and $\pi \rightarrow \pi^*$ interactions with 5.89 and 34.52 kcal mol^{-1} stabilization energy in **DMA** observed are dominant over the rest of the studied

compounds, which was further supported by the results of global reactivity indices and uncovered the greatest chemical potential, electron donating and accepting competency of **DMA**. So, it is concluded that **DMA** and **DAM** exhibit excellent NLO material properties and might be the best candidates for future applications.

Conflicts of interest

The authors declare no conflicts of interest.

Acknowledgements

References

1 A. Rauf, et al., Synthesis, spectroscopic characterization, DFT optimization and biological activities of Schiff bases and their metal (II) complexes, J. Mol. Struct., 2017, 1145, 132–140.

2 A. Rauf, et al., Synthesis, physicochemical elucidation, biological screening and molecular docking studies of a Schiff base and its metal (II) complexes, Arab. J. Chem., 2020, 13, 1130–1141.

3 C. R. Schmid, et al., Synthesis of 2, 3-O-isopropylidene-D-glyceraldehyde in high chemical and optical purity: observations on the development of a practical bulk process, J. Org. Chem., 1991, 56, 4056–4058.

4 B. B. Baldaniya, Synthesis and Characterizations ofN2 (Aryl)-N4, N6-bis (6, 7-dichloro-1, 3-benzothiazol-2-yl)-1, 3, 5-triazine-2, 4, 6-triamines as Biological Potent Agents, Electron. J. Chem., 2010, 7, 210–214.

5 S. V. Bhandari, et al., Design, synthesis and pharmacological screening of novel nitric oxide donors containing 1, 5-diarylpyrazolin-3-one as nontoxic NSAIDs, Eur. J. Med. Chem., 2009, 44, 4622–4636.

6 L. Jiang, et al., Direct and mild palladium-catalyzed aerobic oxidative synthesis of imines from alcohols and amines under ambient conditions, Chem. Commun., 2011, 47, 10833–10835.

7 K. Hoesch and T. v. Zarzecki, Eine neue Synthese aromatischer Ketone. II. Künstliche Darstellung des Maclurins und ihm verwandter Ketone, Berichte Dtsch. Chem. Ges., 1917, 50, 462–468.

8 M. Khalid, et al., NLO potential exploration for D–π–A heterocyclic organic compounds by incorporation of various π-linkers and acceptor units, Arab. J. Chem., 2021, 14, 103295.

9 M. Khalid, et al., Structural modulation of π-conjugated linkers in D–π–A dyes based on triphenylamine dicyanovinylene framework to explore the NLO properties, R. Soc. Open Sci., 2021, 8, 210570.

10 M. Khalid, H. M. Lodhi, M. U. Khan and M. Imran, Structural parameter-modulated nonlinear optical amplitude of acceptor–π–D–π–donor-configured pyrene derivatives: A DFT approach, RSC Adv., 2021, 11, 14237–14250.

11 M. Khalid, et al., Enriching NLO efficacy via designing non-fullerene molecules with the modification of acceptor moieties into ICIF2F: an emerging theoretical approach, RSC Adv., 2022, 12, 13412–13427.

12 M. U. Khan, et al., Influence of acceptor tethering on the performance of nonlinear optical properties for pyrene-based materials with A-π-D-π-D architecture, Arab. J. Chem., 2022, 15, 103673.

13 M. Ashfaq, et al., Synthetic approach to achieve halo imine units: Solid-state assembly, DFT based electronic and non linear optical behavior, Chem. Phys. Lett., 2022, 803, 139843.

14 J. Jia, et al., Effect of intramolecular charge transfer on nonlinear optical properties of chalcone derivatives: a visual description of the charge transfer process, Phys. Chem. Chem. Phys., 2022, 24, 955–965.

15 Y. Shi, et al., Study of ultrafast nonlinear optical response and transient dynamics of pyrene derivatives with intramolecular charge transfer characteristics, Opt. Mater., 2022, 128, 112378.

16 D. Pant, N. Darla and S. Sitha, Roles of various bridges on intramolecular charge Transfers, dipole moments and first hyperpolarizabilities of Donor-Bridge-Acceptor types of organic Chromophores: Theoretical assessment using Two-State model, Comput. Theor. Chem., 2022, 1209, 113583.

17 H. Purandara, et al., Crystal structure elucidation, experimental and computational optical properties of novel acceptor-donor-acceptor organic material: A suitable candidate for nonlinear applications, J. Mol. Struct., 2022, 1248, 131492.

18 D. Pant, N. Darla and S. Sitha, Theoretical assessment of the influences of aromatic bridges on molecular second order nonlinear optical responses of Donor-Bridge-Acceptor types of molecular organic chromophores, Comput. Theor. Chem., 2022, 1207, 113522.

19 M. Khalid, et al., Structural modulation of π-conjugated linkers in D–π–A dyes based on triphenylamine dicyanovinylene framework to explore the NLO properties, R. Soc. Open Sci., 2021, 8, 210570.

20 F. Rasool, et al., Facile synthesis, DNA binding, Urease inhibition, anti-oxidant, molecular docking and DFT studies of 3-(3-Bromo-phenyl)-1-(2-trifluoromethyl-phenyl)-propenone and 3-(3-Bromo-5 chloro-phenyl)-1-(2-trifluoromethyl-phenyl)-propenone, J. Mol. Liq., 2021, 336, 116302.

21 A. Frisch, Gaussian 09W Reference, Wallingford, USA, 2009, p. 25.

22 R. D. Dennington, T. A. Keith and J. M. Millam, GaussView 5.0, Gaussian. Inc., Wallingford, 2008.

23 M. D. Hanwell, et al., Avogadro: an advanced semantic chemical editor, visualization, and analysis platform, J. Cheminformatics, 2012, 4, 1–17.

24 G. A. Zhurko and D. A. Zhurko, ChemCraft, version 1.6, 2009, https//www.Chemcraftprog.com.

25 N. M. O'boyle, A. L. Tenderholt and K. M. Langner, Cclib: a library for package-independent computational chemistry algorithms, *J. Comput. Chem.*, 2008, **29**, 839–845.

26 R. A. T. Lima, *et al.*, Functional and structural characterization of a novel GH3 β-glucosidase from the gut metagenome of the Brazilian Cerrado termite Syntermes wheeleri, *Int. J. Biol. Macromol.*, 2020, **165**, 822–834.

27 T. Lu and F. M. Chen, a multifunctional wavefunction analyzer, *J. Comput. Chem.*, 2012, **33**, 580–592.

28 F. Weinhold, C. R. Landis and E. D. Glendening, What is NBO analysis and how is it useful?, *Int. Rev. Phys. Chem.*, 2016, **35**, 399–440.

29 L. Kara Zaitri and S. M. Mekelleche, Computational study of linear and nonlinear optical properties of substituted thiophene imino dyes using long-range corrected hybrid DFT methods, *Mol. Phys.*, 2020, **118**, 1618508.

30 M. N. Arshad, *et al.*, A potent synthesis and supramolecular synthon hierarchy percipience of (E)-N′-(Napthalen-1-yl-methylene)-benzenesulfonohydrazide and 1-Napthaldehyde: A combined experimental and DFT studies, *J. Mol. Struct.*, 2020, **1221**, 128797.

31 S. H. Sumrra, *et al.*, Synthesis, characterization, and biological screening of metal complexes of novel sulfonamide derivatives: Experimental and theoretical analysis of sulfonamide crystal, *Appl. Organomet. Chem.*, 2020, **34**, e5623.

32 G. Mahalakshmi and V. Balachandran, NBO, HOMO., LUMO analysis and vibrational spectra (FTIR and FT Raman) of 1-Amino 4-methylpiperazine using ab initio HF and DFT methods, *Spectrochim. Acta. A. Mol. Biomol. Spectrosc.*, 2015, **135**, 321–334.

33 M. Adeel, *et al.*, Synthesis, X-ray crystallographic, spectroscopic and computational studies of aminothiazole derivatives, *J. Mol. Struct.*, 2017, **1131**, 136–148.

34 T. Hassan, *et al.*, Development of non-fused acceptor materials with 3D-Interpenetrated structure for stable and efficient organic solar cells, *Mater. Sci. Semicond. Process.*, 2022, **151**, 107010.

35 C.-G. Zhan, J. A. Nichols and D. A. Dixon, Ionization potential, electron affinity, electronegativity, hardness, and electron excitation energy: molecular properties from density functional theory orbital energies, *J. Phys. Chem. A*, 2003, **107**, 4184–4195.

36 R. G. Parr and R. G. Pearson, Absolute hardness: companion parameter to absolute electronegativity, *J. Am. Chem. Soc.*, 1983, **105**, 7512–7516.

37 R. Parthasarathi, V. Subramanian, D. R. Roy and P. K. Chattaraj, Electrophilicity index as a possible descriptor of biological activity, *Bioorg. Med. Chem.*, 2004, **12**, 5533–5543.

38 R. G. Parr, R. A. Donnelly, M. Levy and W. E. Palke, Electronegativity: the density functional viewpoint, *J. Chem. Phys.*, 1978, **68**, 3801–3807.

39 P. Politzer and D. G. Truhlar, *Chemical applications of atomic and molecular electrostatic potentials: reactivity, structure, scattering, and energetics of organic, inorganic, and biological systems*, Springer Science & Business Media, 2013.

40 A. Irfan, A. R. Chaudhry, S. Muhammad and A. G. Al-Sehemi, Exploring the potential of boron-doped nanographene as efficient charge transport and nonlinear optical material: a first-principles study, *J. Mol. Graph. Model.*, 2017, **75**, 209–219.

41 R. Hussain, *et al.*, Enhancement in photovoltaic properties of N, N-diethylaniline based donor materials by bridging core modifications for efficient solar cells, *ChemistrySelect*, 2020, **5**, 5022–5034.

42 M. Khalid, *et al.*, Exploration of second and third order nonlinear optical properties for theoretical framework of organic D–π–D–π–A type compounds, *Opt. Quantum Electron.*, 2021, **53**, 1–19.

43 Z. Demircioğlu, G. Kaştaş, Ç. A. Kaştaş and R. Frank, Spectroscopic, XRD, Hirshfeld surface and DFT approach (chemical activity, ECT, NBO, FFA, NLO, MEP, NPA& MPA) of (E)-4-bromo-2-[(4-bromophenylimino) methyl]-6-ethoxyphenol, *J. Mol. Struct.*, 2019, **1191**, 129–137.

44 Z. Demircioğlu, Ç. A. Kaştaş and O. Büyükgüngör, X-ray structural, spectroscopic and computational approach (NBO, MEP, NLO, NPA, fukui function analyses) of (E)-2-((4-bromophenylimino) methyl)-3-methoxyphenol, *Mol. Cryst. Liq. Cryst.*, 2017, **656**, 169–184.

45 R. Mathammal, K. Sangeetha, M. Sangeetha, R. Mekala and S. Gadheeja, Molecular structure, vibrational, UV, NMR, HOMO-LUMO, MEP, NLO, NBO analysis of 3, 5 di tert butyl 4 hydroxy benzoic acid, *J. Mol. Struct.*, 2016, **1120**, 1–14.

46 B. Khan, *et al.*, Synthetic, spectroscopic, SC-XRD and nonlinear optical analysis of potent hydrazide derivatives: a comparative experimental and DFT/TD-DFT exploration, *J. Mol. Struct.*, 2020, **1200**, 127140.

47 M. Khalid, *et al.*, First principles study of electronic and nonlinear optical properties of A–D–π–A and D–A–D–π–A configured compounds containing novel quinoline–carbazole derivatives, *RSC Adv.*, 2020, **10**, 22273–22283.

48 H. S. Nalwa, T. Watanabe and S. Miyata, Optical Second-Harmonic Generation in Organic Molecular and Polymeric Materials, *Photochem. Photophysics*, 1992, **5**, 103–185.

49 P. N. Prasad and D. J. Williams, *Introduction to nonlinear optical effects in molecules and polymers*, Wiley, New York, 1991, vol. 1.